Supplement Material

Supplementary Figures

Supplementary Figure I. The inhibition of VEGFR-2 activation by PAI-1 is dose-dependent. (A) HUVECs were seeded in wells coated with VN. After achieving 80% confluency, cells were incubated with or without PAI-1-WT as indicated for 4 hr, followed by addition of VEGF (50 ng/mL) for 5 min. Cell lysates were prepared and analyzed for phosphorylated (pVEGFR-2) and non-phosphorylated VEGFR-2. (B) Densitometric analysis of 3 independent experiments. *P<0.05 vs. control; **P<0.05 vs. HUVECs incubated with VEGF in the absence of any PAI-1-WT.

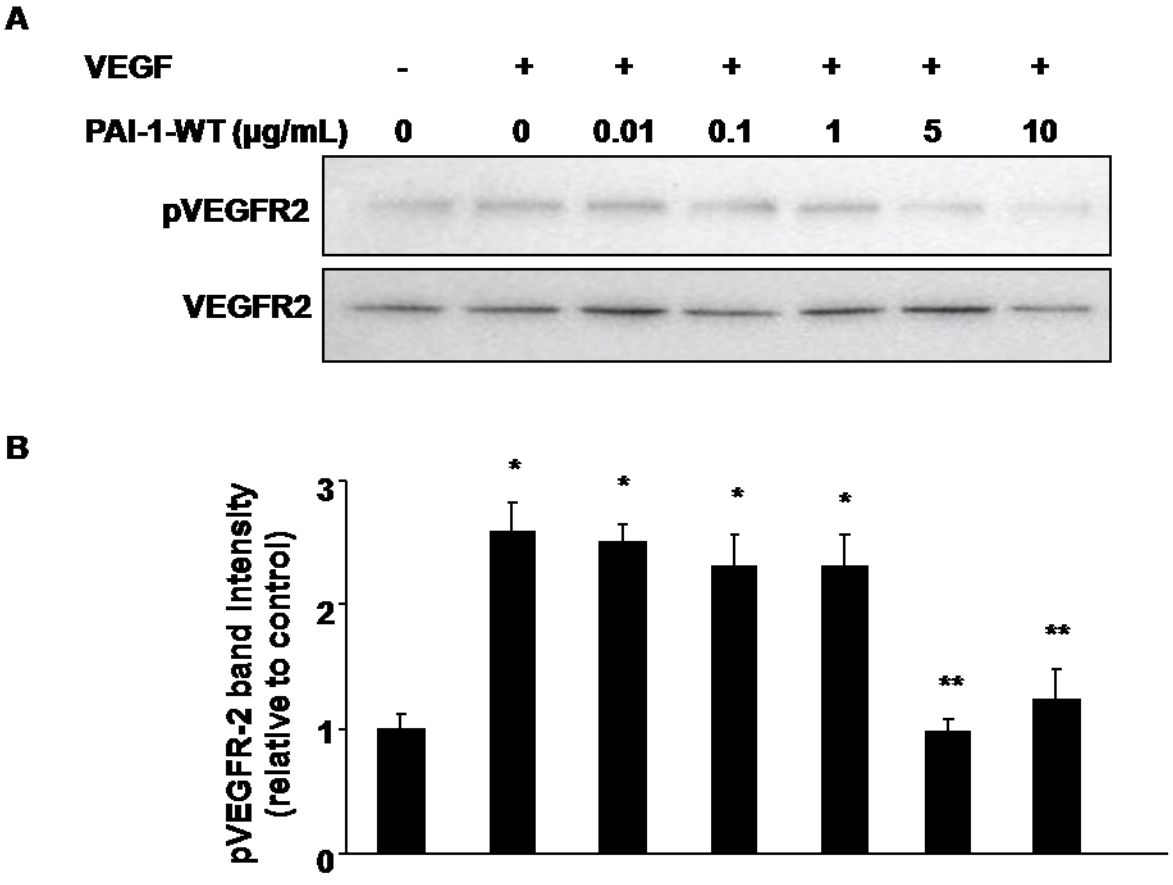

Supplementary Figure II. (A). PAI-1-WT does not bind to immobilized VEGF. (B). PAI-1-WT does not inhibit VEGF binding to VEGFR-2/Fc. Anti-VEGF monoclonal antibody 2C3 (ATCC, which blocks binding of VEGF toVEGFR-2), was used as a positive control.

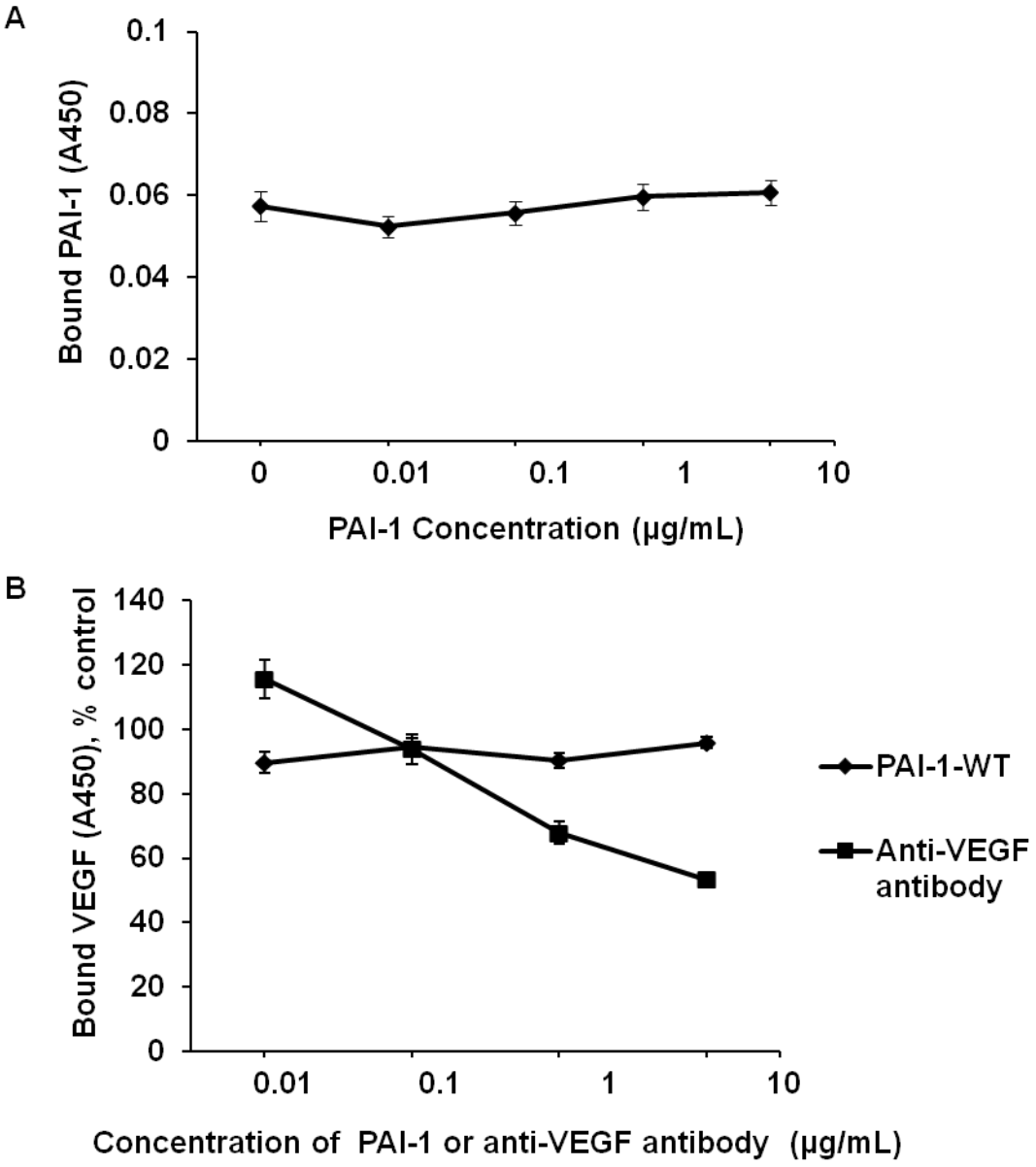

Supplementary Figure III. PAI-1 inhibits VEGFR-2 signaling in human microvascular endothelial cells (HMVECs). (A) PAI-1 inhibits VEGF-induced β_3 integrin-VEGFR-2 complex formation and VEGFR-2 phosphorylation. HMVECs were grown in vitronectin (VN)-coated wells and incubated with vehicle control (-), VEGF (50 ng/mL), or VEGF and PAI-1-WT (10 µg/mL), as indicated. To assess β_3 integrin-VEGFR-2 complex formation, cell lysates were prepared and incubated with resin-bound anti-VEGFR-2 antibody. Captured proteins were analyzed by Western blotting using anti-$\beta_3$integrin anti-VEGFR-2 antibodies. To assess VEGFR-2 phosphorylation, cell lysates were subjected to Western blotting using anti-phosphorylated-VEGFR-2 (pVEGFR-2) antibody. (B) PAI-1-WT inhibits VEGF-induced phosphorylation of p44/p42. HMVECs cell lysates, prepared as described in panel A, were subjected to Western blotting using antibodies specific for phosphorylated-p44/p42 (Phos-p44/p42) and total p44/p42. For both panel A and panel B, representative images and band densitometry analysis of 3 independent experiments are shown. *P<0.05 vs. negative control (HUVECs not treated with either VEGF or PAI-1-WT; i.e. 1st lane and 1st bar of graphs).

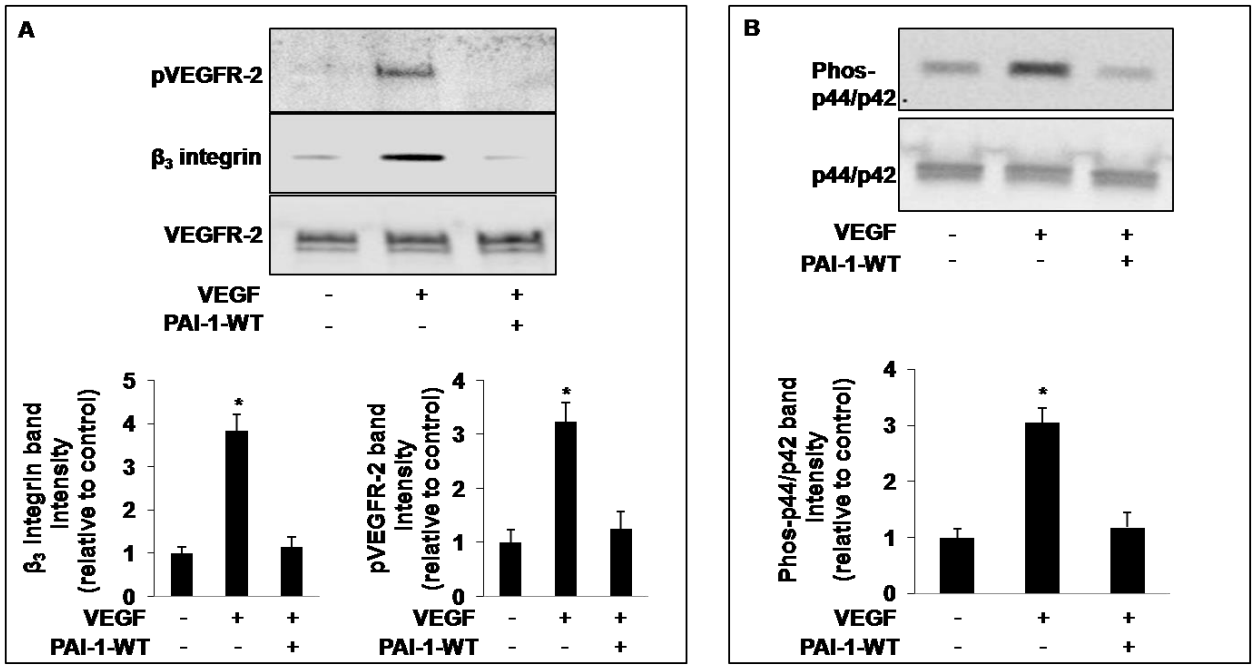

Supplementary Figure IV. Inhibition of VEGFR-2 phosphorylation by PAI-1-AK is blocked by a peptide (D2A-Ala) which inhibits uPAR-integrin binding interactions. HUVECs were grown in vitronectin-coated wells and treated with control peptide or D2A-Ala (100 pM) for 30 min, as shown. Thereafter, HUVECS were treated with vehicle control (-), VEGF (50 ng/mL), VEGF and PAI-1-AK (10 µg/mL), or PAI-1-AK, as shown, after which cell lysates were prepared and analyzed by Western blotting using antibodies specific for phosphorylated VEGFR-2 (pVEGFR-2) and total VEGFR-2. A representative blot is shown as well as band densitometry analysis of 3 independent experiments. Band intensities were normalized to control conditions, which were HUVECs grown in presence of control peptide, but not treated with either VEGF of PAI-1-AK (i.e. 1st bar). *P<0.05 vs. control conditions.

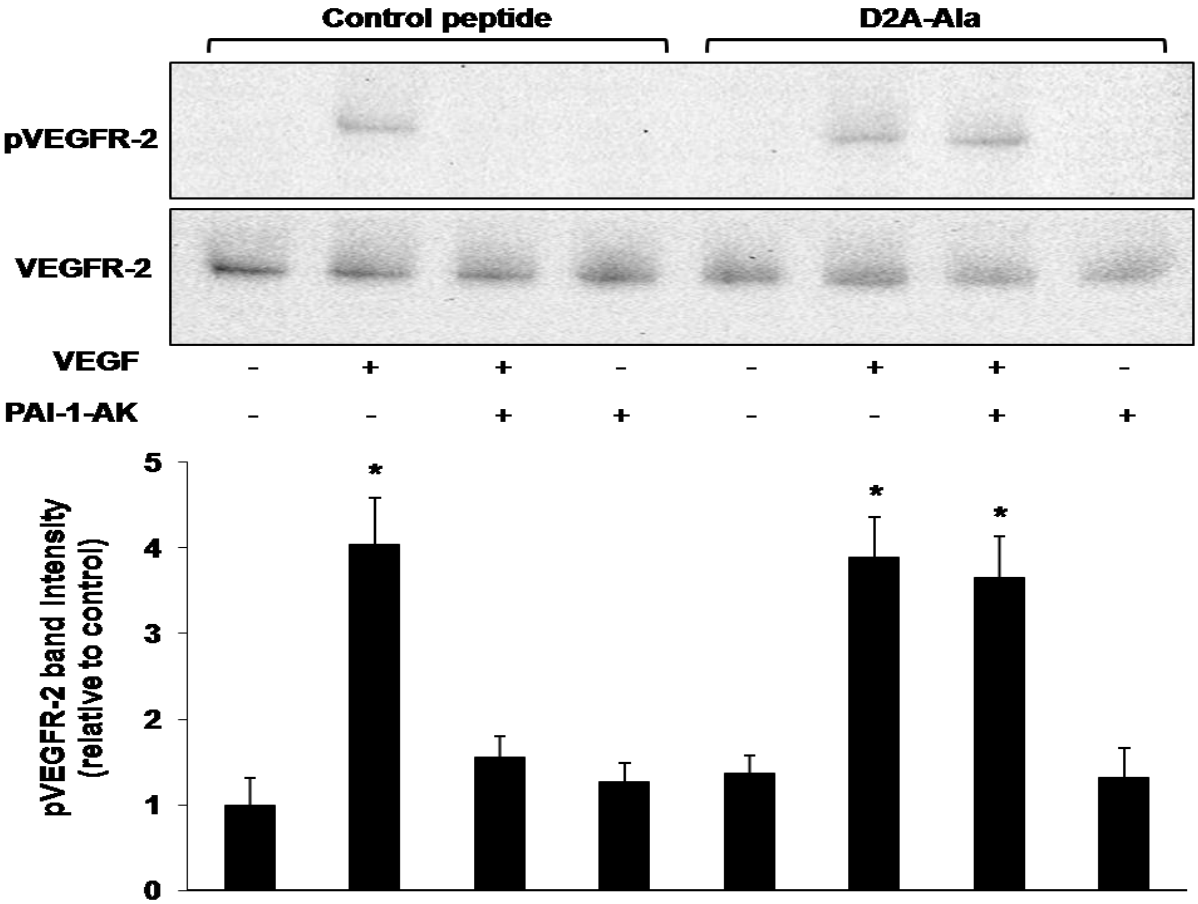

Supplementary Figure V. PAI-1 inhibits VEGF-induced HUVEC migration by binding to very-low-density-lipoprotein receptor (VLDLR). (**A**) The inhibitory effect of PAI-1-AK (but not of PAI-1-WT or PAI-1-R) on VEGF-induced HUVEC migration is blocked by RAP. HUVECs were incubated for 30 min on VN-coated porous membranes in presence (+) of RAP (0.2 μM) or vehicle control (-), after which recombinant PAI-1 (WT, R, or AK forms, each at 10 μg/mL) or vehicle control (-) was added, followed 30 min later by stimulation with VEGF (50 ng/mL, +) or vehicle control (-), as shown. After 24 hr cell migration through pores was measured. (**B**) PAI-1-AKE (which is defective in VN and endocytic receptor binding) does not inhibit VEGF-induced HUVEC migration. (**C**) Ligand-blocking antibody to VLDLR inhibits the anti-VEGF effect of PAI-1-AK. HUVECs were treated sequentially with 1) anti-VLDLR IgG, control (non-immune) IgG, or vehicle control; 2) PAI-1-AK or vehicle control; and 3) VEGF or vehicle control, as shown. Data shown are mean of triplicate experiments and expressed as % of control (1st bar of each graph). *P<0.05 vs. control. Groups other than those denoted by an asterisk did not differ significantly (P>0.05) vs. control.

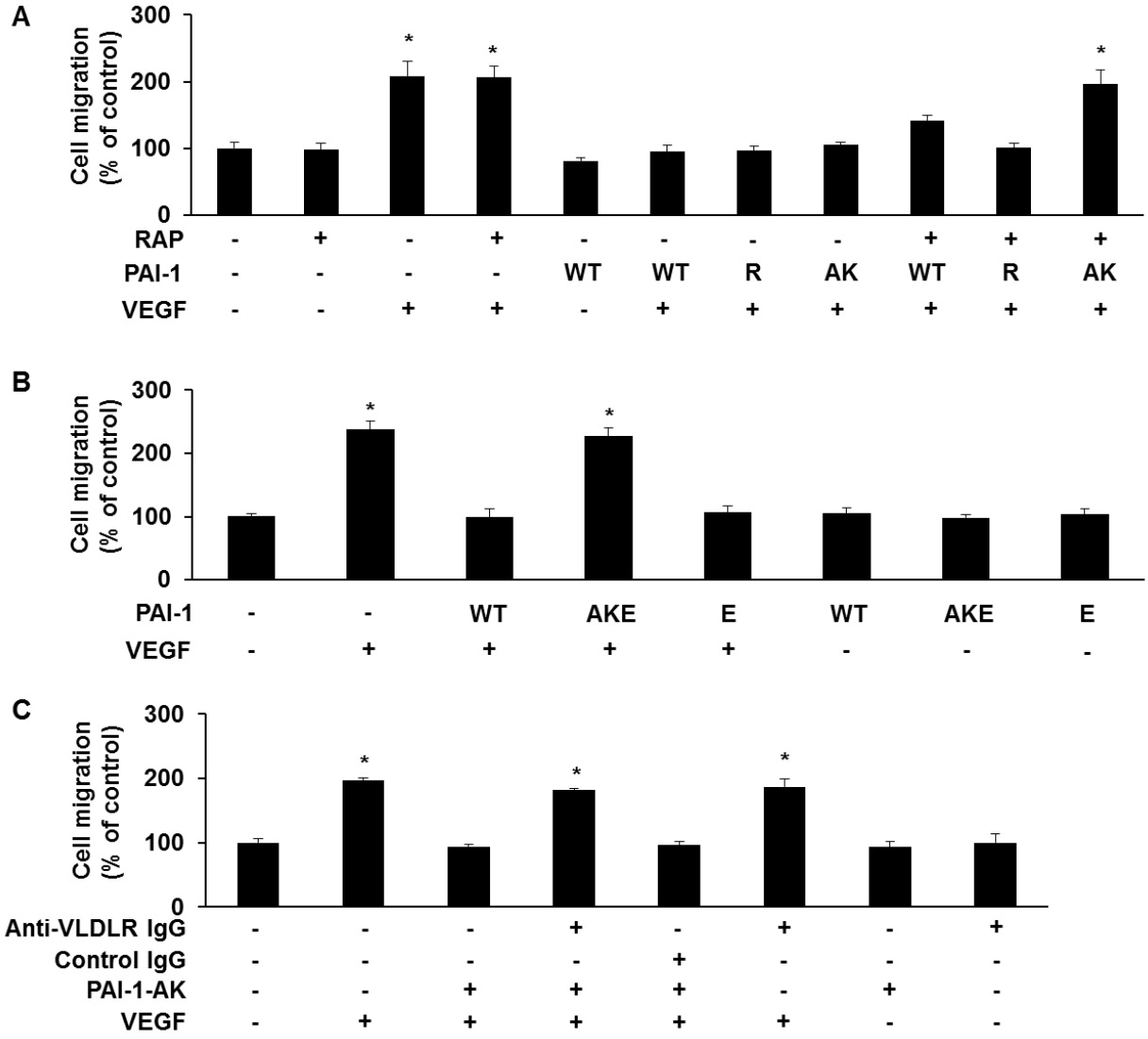

Supplementary Figure VI. Vitronectin (VN) immuno-staining of murine tissues. (A) VN is present in mouse aorta. Thoracic aortic rings from wild-type (WT) mice and *Vn*$^{-/-}$ mice were incubated in serum-free medium for 24 hr, homogenized in RIPA buffer, and centrifuged. Supernatants were subjected to SDS-PAGE (reducing conditions) and Western blotting using anti-VN antibody. A sample of wild-type murine plasma was analyzed as a positive control. To assess for equal loading of wild-type and *Vn*$^{-/-}$ aorta samples, blots were stripped and re-probed with an antibody against β-actin (expected to be present in aorta, but not in plasma). (B) VN is present in Matrigel plugs retrieved from WT mice, but is not detectable in Matrigel plugs retrieved from *Vn*$^{-/-}$ mice. Plugs were retrieved 14 days after insertion. Cross-sections were prepared and subjected to immuno-histochemical staining with anti-VN antibody. Nuclei were stained with methyl green. Brick red color represents positive VN immuno-staining. Data shown are representative of 3 plugs retrieved from each experimental group. Scale bar = 5 µm.

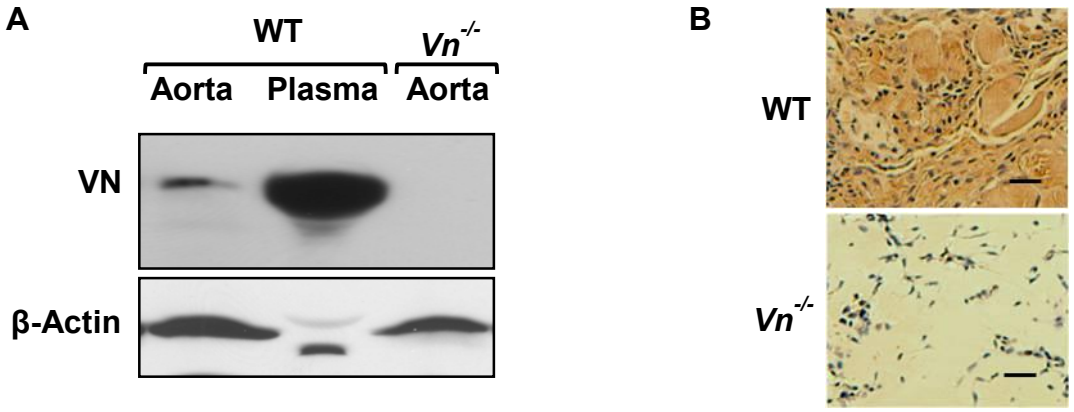

Supplementary Figure VII. High-fat diet induces obesity, hyperglycemia, and increased plasma PAI-1 in mice. Mice were fed high-fat chow (HFC) or normal chow (NC) for 14 weeks, after which (A) body weight, (B) plasma glucose, (C) plasma PAI-1 antigen, and (D) plasma PAI-1 activity were measured (n=6/group); *P<0.05 vs. NC group.